

Quantum interference of electrons in $\text{Nb}_{5-\delta}\text{Te}_4$ single crystals

A. Stolovits* and A. Sherman

Tartu Ülikooli Füüsika Instituut, Riia 142, EE-51014 Tartu, Estonia

R. K. Kremer, H. J. Mattausch, H. Okudera, X.-M. Ren,[†] and A. Simon

Max-Planck-Institut für Festkörperforschung, Heisenbergstrasse 1, D-70569 Stuttgart, Germany

J. R. O'Brien

Quantum Design, 6325 Lusk Boulevard, San Diego, CA 92121

(Dated: March 23, 2022)

The compound $\text{Nb}_{5-\delta}\text{Te}_4$ ($\delta = 0.23$) with quasi-one-dimensional crystal structure undergoes a transition to superconductivity at $T_c = 0.6\text{--}0.9$ K. Its electronic transport properties in the normal state are studied in the temperature range 1.3–270 K and in magnetic fields up to 11 T. The temperature variation of the resistivity is weak ($< 2\%$) in the investigated temperature range. Nonmonotonic behavior of the resistivity is observed which is characterized by two local maxima at $T \sim 2$ K and ~ 30 K. The temperature dependence of the resistivity is interpreted as an interplay of weak localization, weak antilocalization, and electron-electron interaction effects in the diffusion and the Cooper channel. The temperature dependence of the dephasing time τ_φ extracted from the magnetoresistance data is determined by the electron-phonon interaction. The saturation of τ_φ in the low-temperature limit correlates with T_c of the individual crystal and is ascribed to the scattering on magnetic impurities.

PACS numbers: 72.15.Rn, 74.70.Ad, 72.15.Lh, 72.10.Di, 74.62.Dh

I. INTRODUCTION

In disordered metals the coherence of the conduction electrons may extend over large distances and exceed the mean free path by several orders of magnitude. This large scale coherence manifests itself in interference effects such as weak localization, interference corrections to electron-electron interaction and various mesoscopic phenomena.^{1,2} In general, the temperature dependence of the dephasing time τ_φ is governed by electron-electron and electron-phonon interaction. In disagreement with the standard theory of electron dephasing,³ a saturation of τ_φ in the low-temperature limit has been observed in numerous experiments. It was suggested that this saturation is universal and reflects fundamental properties of disordered conductors.^{4,5} Various mechanisms for the saturation behavior have been discussed, including effects of magnetic impurities, tunneling two-level systems, electron heating, and separated superconducting grains⁶ (see Refs. 7,8).

Recently the character of the disorder and its influence on τ_φ have become an important issue of research. Weak localization studies of differently prepared PdAg films show that the microscopic structure of disorder determines the interaction of the electrons with the phonons.⁹ The nature of the scattering potential plays a crucial role in the Sergeev-Mitin electron-phonon interaction theory.¹⁰ While in dirty systems the scattering on vibrating impurities results in a T^4 dependence of the electron-phonon scattering rate τ_{ep}^{-1} , scattering on a static potential leads to $\tau_{ep}^{-1} \sim T^2$. Disorder also influences the saturation value τ_0 of the dephasing time. For example, Lin *et al.* found that annealing of moderately disordered three-

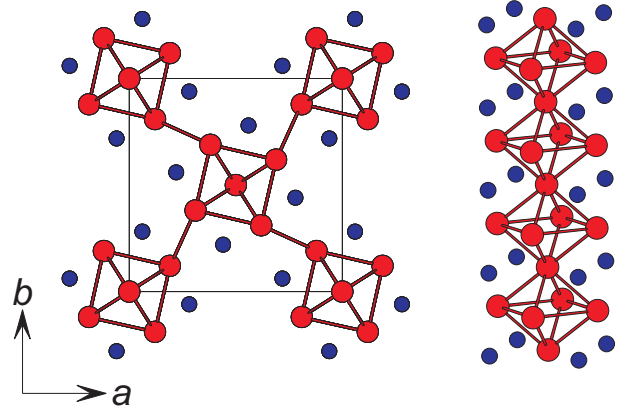


FIG. 1: Projection of the Nb_5Te_4 structure along the c -axis of the tetragonal unit cell (left) and perspective view of its single chain of Nb_6 octahedra (right). Large circles indicate Nb atoms, small circles represent Te atoms.

dimensional polycrystalline metals raises τ_0 .¹¹ This result can be explained in terms of two-level systems associated with the grain boundaries. However, annealing effects have not been observed in strongly disordered samples.¹¹ To further investigate disorder effects, systems in which the crystallinity can be tuned in a broad range are desirable. Single crystalline systems with disorder, e. g. emerging from vacancies, which exhibit quantum interference effects are potential candidates for such studies.

In this paper we present electron transport studies on single crystals of $\text{Nb}_{5-\delta}\text{Te}_4$. $\text{Nb}_{5-\delta}\text{Te}_4$ belongs to the growing family of compounds crystallizing with the tetragonal Ti_5Te_4 structure-type (space group $I4/m$).¹²

For a list of presently known compounds with this structure-type see Ref. 13. The basic elements of the structure are compressed Ti_6Te_8 clusters which condense to form infinite Ti_5Te_4 chains. These chains are linked through Ti-Te and Ti-Ti contacts (see Fig. 1). Ti_5Te_4 , Nb_5Te_4 , Mo_5As_4 , Nb_5Sb_4 , and $\text{Nb}_5\text{Se}_2\text{S}_2$ are reported to be metals.^{14,15,16} Among them Nb_5Sb_4 and $\text{Nb}_5\text{Se}_2\text{S}_2$ are superconductors with critical temperatures $T_c = 8.6$ K and 3.4 K, respectively.^{15,17} Nb_5Te_4 and Ti_5Te_4 were reported to behave as normal metals down to 1.1 K.¹⁷ Recently, a monoclinic form of $\text{Nb}_{4.7}\text{Te}_4$ has been synthesized using a chemical transport reaction.¹⁸

In this work we found that $\text{Nb}_{5-\delta}\text{Te}_4$ is a bulk superconductor with $T_c = 0.6\text{--}0.9$ K. In the normal state quantum interference effects determine the electronic transport properties in a broad temperature range. The observed nonmonotonic behavior of the temperature dependence of the resistance and the low-temperature positive magnetoresistance are interpreted in terms of weak localization and electron-electron interaction effects in disordered conductors. The temperature dependence of the dephasing time τ_φ is determined by electron-phonon interaction. Saturation of the dephasing time at low temperatures is ascribed to scattering on magnetic impurities.

II. EXPERIMENTAL

$\text{Nb}_{5-\delta}\text{Te}_4$ single crystals were prepared by chemical vapor transport from powders of the elements Nb (Johnson Matthey Inc. 99.99% metals basis, excluding Ta, Ta < 500 ppm) and Te (Johnson Matthey Inc. 99.99%) in evacuated silica tubes with I_2 used as a transport agent. The samples were annealed for 1 day at 750°C , the following 30 days at 980°C , and then were slowly cooled to room temperature. X-ray powder-diffraction patterns were collected with a Stoe diffractometer using ($\text{Cu } K_{\alpha 1}$ radiation). They show a body-centered tetragonal unit cell with lattice parameters $a = 10.234(1)$ Å and $c = 3.7021(6)$ Å which are in agreement with those observed by Selte and Kjekshus.¹² Energy dispersive x-ray analysis carried out on the three crystals used for the resistance measurements reveals a Nb deficiency of $\delta = 0.23(4)$. A single crystal x-ray diffraction measurement with a Stoe image plate detector system was carried out on a small crystal. It shows that the Nb deficiency is associated with the outer site of the Nb octahedral chains (Wyckoff position $8h$). Single crystal x-ray measurements performed on the three crystals used for the resistance measurements gave lattice parameters in good agreement with the powder diffraction data.

The heat capacity of a 6.3 mg crystal was measured in a Quantum Design PPMS relaxation calorimeter in the temperature range 0.3–5 K and external fields of 0 T and 9 T. The sample was attached with a minute amount of Apiezon vacuum grease to the calorimeter platform the heat capacity of which was determined in a separate run

and subtracted afterwards.

For resistance measurements needle-like crystals with the needle axis collinear with the crystallographic c -axis were selected. Crystals were 3–5 mm long with cross section of $0.005\text{--}0.05$ mm². Four electrical contacts were placed along the needle at distances of ~ 2 mm with the two outer contacts as the current contacts such that the electrical current was directed along the c -axis.

Crystals stored in air get covered by a high-resistive oxide layer. Low-resistance ohmic contacts can be achieved after this layer has been etched off with an Ar plasma in a vacuum chamber followed by the immediate deposition of the gold contact pads through a shadow mask. Similar good contacts can also be made by gluing gold wires with silver epoxy resin on a crystal surface freshly cleaved in an argon atmosphere. The results do not depend on the way contacts have been applied.

The resistance was measured by a dc four-probe technique using a high resolution nanovoltmeter (7 1/2 digits) and a Keithley 2400 current source. Measurements were performed using a variable temperature Oxford ⁴He cryostat with a superconducting magnet. The rotatable sample holder with the rotation axis perpendicular to the magnetic field allows us to align the crystal either perpendicular or nearly parallel to the magnetic field. Magnetoresistance was measured at constant temperature in fields up to 11 T. The superconducting transition and its dependence on the magnetic field was measured in a home-built single shot ³He refrigerator. The bias currents were chosen such that the power dissipated in the sample remained below 30 pW and 2 μW for the measurements in the ³He and the ⁴He measurements systems, respectively.

III. RESULTS AND DISCUSSION

A. Superconductivity

A total of six crystals was checked for superconductivity by resistance measurements. All investigated samples show a transition to superconductivity with critical temperatures in the range 0.60–0.88 K and transition widths between 0.012–0.18 K. A typical resistive transition is shown in Fig. 2(c). Measurements in magnetic fields reveal a linear dependence of the upper critical field $H_{c2}(0)$ as a function of temperature down to 0.35 K, with a slope of $dH_{c2}/dT = -1.2$ T/K.

The heat capacity measured in zero field is characterized by an anomaly typical for a transition to superconductivity (Fig. 2(b)). The anomaly disappears in a field of 9 T. In the range 0.3–2 K the heat capacity can be well described by a polynomial $C_p = \gamma T + \beta T^3$, where the linear and cubic terms are electronic and lattice contributions, respectively (Fig. 2(a)). The fit yields the Sommerfeld term $\gamma = 17.29$ μJ/g K², and the phonon term $\beta = 1.027$ μJ/g K⁴ corresponding to the Debye temperature $\Theta_D = 259$ K. The superconducting anomaly

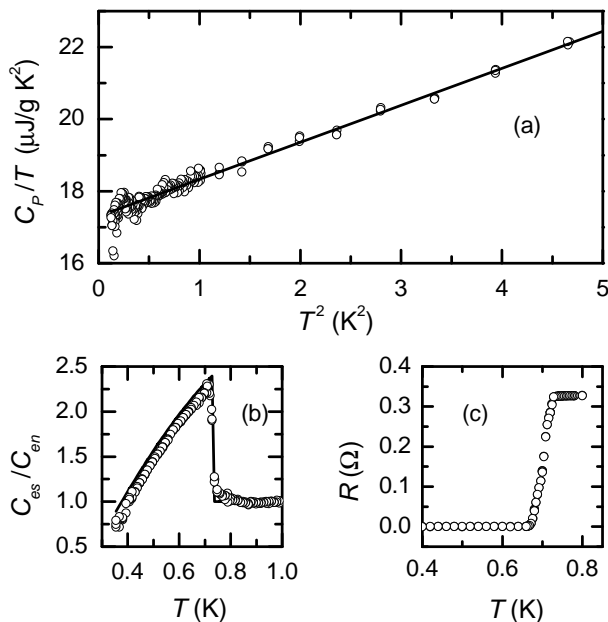


FIG. 2: (a) Specific heat C_p of $\text{Nb}_{5-\delta}\text{Te}_4$ measured in a magnetic field of 9 T plotted as C_p/T vs T^2 . The symbols represent the experimental data and the solid line a fit to the equation $C_p = \gamma T + \beta T^3$ with $\gamma = 17.29 \mu\text{J/g K}^2$ and $\beta = 1.027 \mu\text{J/g K}^4$. (b) The ratio of the electronic heat capacity in the superconducting state C_{es} to that in the normal state C_{en} as a function of temperature. The solid line is the heat capacity anomaly expected for a BCS superconductor with $T_c = 0.73$ K. (c) The superconducting transition of Nb09 (see TABLE I) measured from the electrical resistance at 0 T.

within experimental errors agrees well with the anomaly expected for a BCS-type superconductor. Resistivity and heat capacity results clearly prove that $\text{Nb}_{5-\delta}\text{Te}_4$ is a bulk superconductor.

The electronic density of states at the Fermi level ν was calculated from the Sommerfeld term using the formula¹⁹ $\gamma = \pi^2 \nu k_B^2 (1 + \lambda)/3$, where k_B is the Boltzmann constant. The electron-phonon coupling constant $\lambda = 0.44$ was estimated from the McMillan empirical formula¹⁹

$$\lambda = \frac{1.04 + \mu^* \ln(\Theta_D/1.45T_c)}{(1 - 0.62\mu^*) \ln(\Theta_D/1.45T_c) - 1.04}, \quad (1)$$

with the Coulomb pseudopotential $\mu^* = 0.13$, which is typical for the transition metals. In $\text{Nb}_{5-\delta}\text{Te}_4$ we obtain $\nu = 1.59 \times 10^{47} \text{J}^{-1} \text{m}^{-3}$, which is comparable to the density of states in good metals such as silver, copper, and gold.

B. Electrical Resistivity

The temperature dependence of the resistivity was measured on six crystals. All samples show resistivities between 200–300 $\mu\Omega \text{cm}$ (see Table I) and a weak variation with temperature (less than 2% in the range of 2–

270 K, see Fig. 6). This finding points to strong scattering of conduction electrons. This is also reflected in the electron diffusion constant D ($\approx 1 \text{ cm}^2/\text{s}$) and a low Hall mobility. The diffusion constant was determined from the temperature dependence of the critical magnetic field using $D = -4k_B/[\pi e (dH_{c2}/dT)]$, where e is the electron charge.²⁰ An alternative estimation of D from the resistivity ρ_0 using the Einstein relation $1/\rho_0 = e^2 D \nu$ gives $D = 0.9\text{--}1.2 \text{ cm}^2/\text{s}$, which is consistent with the value determined from $H_{c2}(T)$ to within 20% (see Table I). The agreement is reasonable considering uncertainties in ρ_0 and ν . As being more reliable, the value of D estimated from the critical magnetic field measurements will be used in the analyses below. The Hall constant is negative indicating that electrons contribute to the charge transport. The Hall mobility is low, $0.25 \text{ cm}^2/(\text{Vs})$, which in the free electron model gives an electron mean free path of $\ell \simeq 2 \text{ \AA}$ of the order of interatomic distances. The origin of strong electron scattering in $\text{Nb}_{5-\delta}\text{Te}_4$ is an open question. The Nb deficit is definitely essential, however deformations of the low-dimensional structure may also contribute to the scattering.

A closer inspection of the temperature dependence of the resistance reveals qualitatively different behavior above ~ 50 K with either positive or negative temperature coefficients (see Figure 6(a)). The magnetoresistance behavior and the temperature dependence of the resistance of three representative samples Nb10, Nb19, and Nb09 have been studied in detail and the analysis is described in the following.

1. Magnetoresistance

Figure 3 shows a typical dependence of the resistance on the magnetic field measured for temperatures between 1.3 K and 13 K. The small positive magnetoresistance ($< 0.3\%$) with a minimum centered at zero magnetic field, which broadens as the temperature is increased, is a typical fingerprint of quantum interference effects of the conduction electrons.¹ The positive magnetoresistance is expected in disordered superconductors containing heavy elements in which both the scattering on virtual Cooper pairs and weak antilocalization of conduction electrons induced by spin-orbit scattering are essential. We found that the magnetoresistance is independent of the orientation of the magnetic field. This result is rather unexpected in view of the anisotropic crystal structure. We tentatively ascribe this finding to averaging effects caused by strong electron scattering.

In the following we compare our magnetoresistance data with results of a theory treating three-dimensional quantum interference corrections to resistivity. In the limit of low fields the relative change of the resistance is

TABLE I: Values of relevant parameters for Nb_{5-δ}Te₄ samples. T_c is the superconducting temperature (midpoint of resistive transition), D is the diffusion constant determined from $H_{c2}(T)$, and ρ_0^* is the resistivity measured at 300 K. ρ_0 , c_{MT} , and k_C are fitting parameters of the magnetoresistance; K , n , and τ_0^{-1} describe the temperature dependence of the dephasing time; k_C^* , L , p , and the electron screening parameter \tilde{F} were determined from the temperature dependence of the resistance.

Sample	T_c (K)	D (cm ² /s)	ρ_0^* ($\mu\Omega$ cm)	ρ_0 ($\mu\Omega$ cm)	c_{MT}	k_C	k_C^*	K (s ⁻¹ K ⁻ⁿ)	n	τ_0^{-1} (s ⁻¹)	\tilde{F}	L	p
Nb10	0.79	0.924	241	249	0.768	0.379	0.371	7.75×10^8	2.45	1.77×10^{10}	0.048	90×10^{-6}	1.28
Nb19	0.88	0.883	231	254	0.730	0.668	0.392	4.39×10^8	2.68	0.58×10^{10}	-0.323	71×10^{-6}	1.37
Nb09	0.70	0.890	304	294	0.769	0.348	0.314	9.52×10^8	2.42	2.61×10^{10}	-0.234	129×10^{-6}	1.19

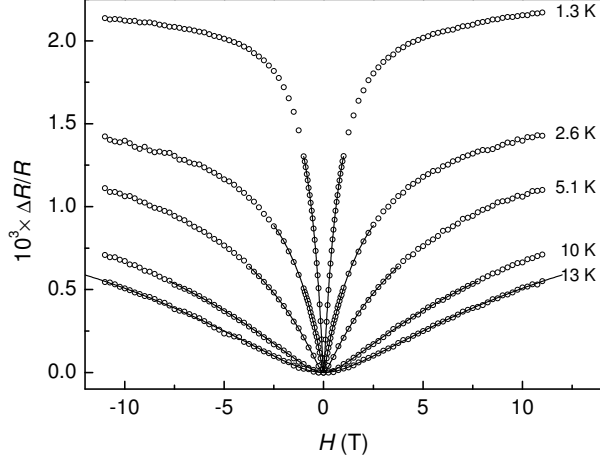


FIG. 3: The normalized magnetoresistance $\Delta R/R = [R(H) - R(0)]/R(0)$ in Nb19 (see TABLE I) versus the magnetic field for several temperatures. The symbols are the experimental data and the lines are the fits with Eq. (2) for the three-dimensional quantum interference corrections.

expressed by the equation^{21,22}

$$\frac{R(H) - R(0)}{R(0)} = A \frac{e^2}{2\pi^2\hbar} \sqrt{\frac{eH}{\hbar}} f_3\left(\frac{4eD\tau_\varphi H}{\hbar}\right) + BH^2, \quad (2)$$

where \hbar is the Planck constant and $f_3(1/x) = 2(\sqrt{2+x} - \sqrt{x}) - [(0.5+x)^{-1/2} + (1.5+x)^{-1/2}] + (2.03+x)^{-3/2}/48$.²³ In Eq. (2), the first term with the prefactor $A = \rho_0/2$ describes weak antilocalization in the limit of strong spin-orbit scattering, $\tau_\varphi^{-1} \ll \tau_{so}^{-1}$, where τ_{so}^{-1} is the spin-orbit scattering rate. In superconductors for $T > T_c$ the scattering on virtual Cooper pairs, the Maki-Thompson-Larkin effect, is also described by the first term in Eq. (2) with a temperature-dependent prefactor $A = \rho_0 c_{MT} \beta(T/T_c)$. Here β is the function tabulated in Ref. 24 and $c_{MT} = 1$ and 0.25 in the limits of weak and strong spin-orbit scattering, respectively.²² This expression is valid for magnetic fields $H \ll k_B T/eD$. Expressions for larger fields have been derived for the two-dimensional case.^{25,26} For the three-dimensional case, results for an extended range of fields have only been analyzed numerically for an Mg₆₇Zn₃₃ alloy sample.²⁷

In the field limit set by the Maki-Thompson-Larkin

effect, $H \ll k_B T/eD$, contributions of the classical magnetoresistance and electron-electron interaction are described by the quadratic term in Eq. (2). The magnetoresistance due to the electron-electron interaction in the Cooper channel is negative and diverges as T approaches T_c . Its contribution is described by the parameter²²

$$B = -8.49 \times 10^{-3} \left(\frac{D}{\hbar k_B T} \right)^{3/2} \frac{e^4 \rho_0 k_C}{\ln(T/T_c)}, \quad (3)$$

with $k_C = 1$ and 0.25 in the limit of weak and strong spin-orbit scattering, respectively. In fields $H \ll k_B T/g\mu_B$ the electron-electron interaction in the diffusion channel is described by the coefficient

$$B = 9.5 \times 10^{-4} \rho_0 \tilde{F} \sqrt{\frac{k_B T}{\hbar D}} \left(\frac{g\mu_B}{k_B T} \right)^2, \quad (4)$$

where μ_B is the Bohr magneton and g is the gyromagnetic ratio.²⁸ The electron-screening parameter \tilde{F} approaches 1 in the limit of complete screening and 0 if screening is negligible. In superconductors due to the exchange with virtual phonons, negative values of \tilde{F} are expected.^{1,29}

In the magnetic field range $|H| \leq 0.5 k_B T/eD$ the magnetoresistance data were fitted to Eq. (2) using A , B , and τ_φ as fitting parameters. The fits shown as solid lines in Fig. 3 are in good agreement with the experimental data for all temperatures. The temperature dependence of A , B , and τ_φ is displayed in Fig. 4 and 5. A is positive and increases as the temperature decreases below 9 K. The temperature dependence of A is well described by the formula

$$A = \rho_0 [c_{MT} \beta(T/T_c) + 1/2], \quad (5)$$

with the Maki-Thompson-Larkin correction and weak antilocalization due to strong spin-orbit scattering as first and second terms, respectively. The fit parameters ρ_0 coincide within 10% with the measured values of the electrical resistivities (see Table I). Below, the fitted values for ρ_0 will be used for the description of the temperature dependence and the electron-electron interaction in the Cooper channel. For strong spin-orbit scattering, c_{MT} is expected to be 0.25 (see above). The fits rather give

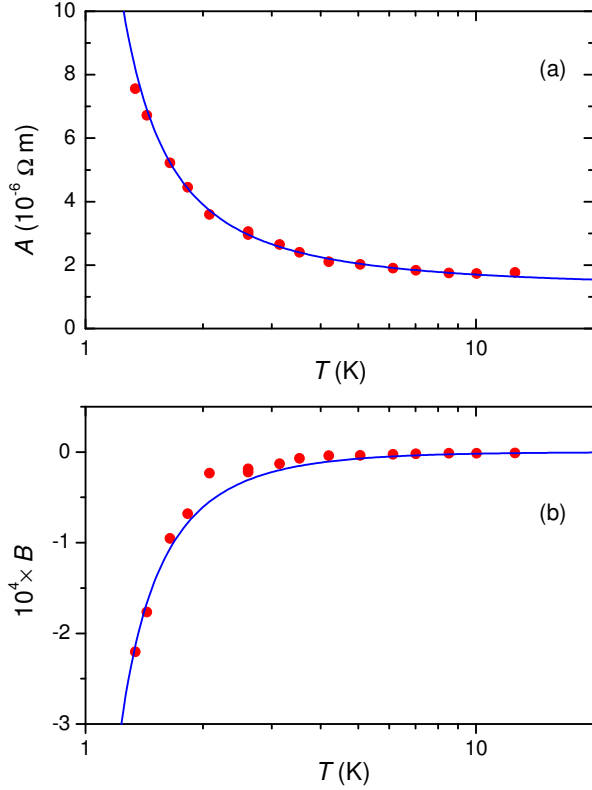


FIG. 4: Temperature dependence of the coefficient A (the upper panel) and B (the lower panel) for sample Nb19 (see TABLE I). Solid lines are the best fit for A and B with Eq. (5) and (3), respectively.

$0.730 < c_{MT} < 0.769$ indicating that the strong spin-orbit scattering limit for the Maki-Thompson-Larkin correction is not realized. Such a situation has often been observed in two- and three-dimensional systems.^{30,31}

B is negative, and its characteristic temperature dependence (see Fig. 4(b)) allows us to identify the origin of the second term in Eq. (2) with the electron-electron interaction in the Cooper channel. The single-parameter fit with Eq. (3) is in good agreement with the experimental data. As in the case of the Maki-Thompson-Larkin correction, the value of the fitting parameter k_C (see Table I) lies between the strong and weak spin-orbit scattering limits.

Figure 5 shows the temperature dependence of τ_φ for samples Nb09, Nb10, and Nb19. The solid lines correspond to fits with the formula

$$\tau_\varphi^{-1} = KT^n + \tau_0^{-1}, \quad (6)$$

with the fitting parameters τ_0^{-1} , K , and n listed in Table I. In Eq. (6) the exponent $n \approx 2.5$ indicates that the temperature dependence of τ_φ^{-1} arises from electron-phonon interaction. A similar temperature dependence with comparable exponents has been observed for NbC, Sb, and Pd₆₀Ag₄₀.^{9,32,33} Dephasing due to electron-

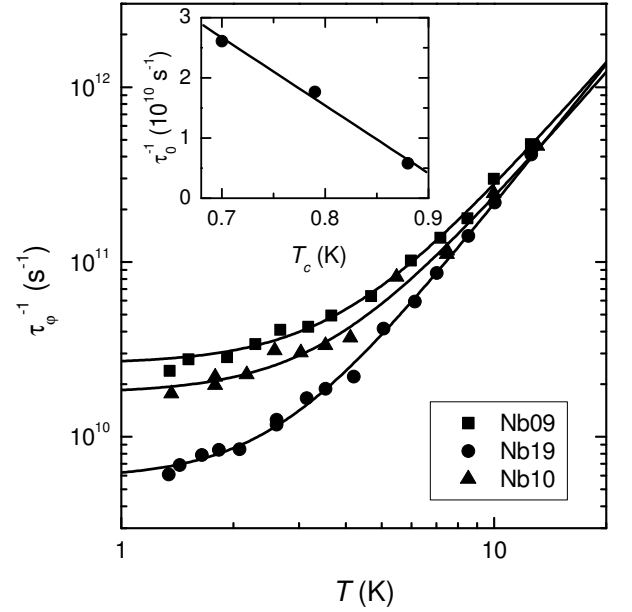


FIG. 5: The dephasing rate τ_φ^{-1} vs. temperature for samples Nb09, Nb10, and Nb19 (see TABLE I). Symbols represent experimental data and the solid lines are the best fit with Eq. (6). Inset: τ_0^{-1} dependence on the superconducting transition temperature.

electron interaction with small energy transfer is also described by a power law but with a smaller exponent, $n = 3/2$, and the coefficient^{34,35}

$$K = \frac{k_B^{3/2}}{12\sqrt{2}\pi^3\hbar^{5/2}\nu D^{3/2}}. \quad (7)$$

Numerical estimates with this formula give a dephasing rate which is more than two orders of magnitude smaller than that observed in the experiment. Therefore, as is often the case in three-dimensional systems, this mechanism can be neglected for Nb_{5-δ}Te₄.⁷

Deviations of $\tau_\varphi^{-1}(T)$ from the power law are observed below 5 K and are described by the parameter τ_0^{-1} . The fitted values for τ_0^{-1} correlate with the critical temperatures (see inset in Fig. 5). This points to scattering on magnetic impurities which decreases both T_c and the dephasing time. The spin-flip scattering rate τ_s^{-1} is proportional to the concentration of magnetic impurities x_{mag} according to³⁶

$$\frac{1}{\tau_s} = \frac{x_{\text{mag}}}{\pi\hbar\nu} \frac{\pi^2 S(S+1)}{\pi^2 S(S+1) + \ln^2(T/T_K)}, \quad (8)$$

where S is the impurity spin and T_K is the Kondo temperature. For impurities with $S > 3/2$ and $T_K < 0.3$ K we obtain $x_{\text{mag}} = 9 \times 10^{-6}$, 30×10^{-6} , and 42×10^{-6} per host atom for Nb19, Nb10, and Nb09 respectively. These concentrations correlate with the purity of the starting materials used for the sample preparation. Additionally, we carried out temperature dependent magnetization measurements on Nb_{5-δ}Te₄. These reveal a

Curie type susceptibility contribution with a Curie constant which is consistent with these impurity estimates if we assume Fe^{3+} ions ($S = 5/2$) as major impurities.

The effect of the magnetic impurities on T_c is characterized by the slope dT_c/dx_{mag} . In $\text{Nb}_{5-\delta}\text{Te}_4$ we have $dT_c/dx_{\text{mag}} = -5.3 \times 10^3$, which is of the same order of magnitude as observed for Zn-Ni, Zn-Co, and Al-Mn alloys.³⁷

Other mechanisms of the dephasing saturation can be excluded based on experimental data. Electron scattering by the exchange of superconducting fluctuations modifies the temperature dependence of τ_φ near T_c . In various systems this effect manifests itself either through a negative temperature coefficient^{31,38,39,40} or a saturation³⁹ of $\tau_\varphi(T)$. In the latter case an increase in τ_0^{-1} with increasing T_c is expected which is not seen in the experiments. This result is also in line with the conclusion that contribution of the electron-electron interaction in τ_φ is negligible.

Nonequilibrium effects of the conduction electrons can lead to saturation of τ_φ in several cases.^{7,41} Measurements of R and τ_φ at different bias currents show that heating effects are not important in our experiment. Besides, the internal thermometers associated with the Maki-Thompson-Larkin effect and the electron-electron interaction in the Cooper channel (Fig. 4) follow the variation of the external temperature, while τ_φ saturates. This also indicates that for the chosen measuring parameters the system is in thermal equilibrium.

We note that our τ_0 values agree with the scaling relation for this parameter found by Lin and Kao for numerous three-dimensional polycrystalline alloys with small diffusion constant ($D=0.1\text{--}10\text{ cm}^2/\text{s}$).⁴ However, in view of the magnetic impurities found in our samples the agreement rather appears to be accidental. Investigations crystals with a reduced impurity level are necessary to compare the saturation behavior of τ_φ in single- and polycrystalline materials.

2. Temperature dependence of resistance

Figure 6 displays the temperature dependence of the resistance for $T > T_c$. Up to 270 K, the resistance varies by less than 2% which indicates that the contribution of the electron-phonon scattering to the resistivity is largely suppressed. A closer inspection reveals that the temperature dependence is nonmonotonic and characterized by one maximum around 2 K and a second maximum/hump between 20 K and 40 K. We ascribe this behavior to an interplay of weak localization and electron-electron interaction effects, some of which also contribute to the magnetoresistance. At $T > 50$ K the temperature dependence is sample dependent. Typical behaviors are illustrated by samples Nb09, Nb10, and Nb19 in Fig. 6(a). While in Nb09 a negative temperature coefficient extends

up to room temperature, Nb10 shows a metallic behavior with a positive temperature coefficient at all temperatures. Nb19 with a resistance minimum at 130 K falls between these two limiting cases.

We begin the data analysis with the low-temperature region around the first maximum. We associate it with the interplay of the superconducting fluctuation effects and the electron-electron interaction in the diffusion channel. For these temperatures the weak antilocalization is suppressed because of the saturation of τ_φ . In the range 1.2–4.2 K the experimental data are well fitted by the formula^{1,21}

$$\frac{R(T)}{R(T_m)} = \frac{e^2}{2\pi^2\hbar}\rho_0 \left\{ \sqrt{\frac{k_B T}{\hbar D}} \left[-F_d - \frac{0.915k_c}{\ln(T/T_c)} \right] - \frac{4}{3\pi^2} c_{\text{MT}} I_{\text{MT}}(T/T_c, \tau_\varphi) \right\} + \sqrt{\frac{1}{4\tau_\varphi(T)D}} \} + R_0. \quad (9)$$

The first term in Eq. (9) corresponds to the electron-electron interaction in the diffusion channel with $F_d = 0.915(2/3 - 3\tilde{F}/4)$. The electron-electron interaction in the Cooper channel, the Maki-Thompson-Larkin correction, and the weak antilocalization, also observed in the magnetoresistance, are described by the second, third and fourth terms, respectively. I_{MT} is a triple integral (see Eq. (56) in Ref. 42), which determines the dependence of the Maki-Thompson-Larkin correction on T/T_c and τ_φ . The values of the fitting parameters \tilde{F} , k_C are listed in Table I. The values of k_C determined from $R(T)$ and $R(H)$ are consistent with each other. As expected for superconductors, \tilde{F} is negative in Nb09 and Nb19. Their values -0.234 and -0.323 for Nb09 and Nb19, respectively, are close to those found, for example, in $\text{Ti}_{1-x}\text{Sn}_x$ and $\text{Ti}_{1-x}\text{Ge}_x$ alloys which show higher critical temperatures.²⁹ In Nb10 \tilde{F} is larger and positive, $\tilde{F} = 0.048$. We attribute this to the Boltzmann transport term which extends to lower temperatures in this sample and is not included in Eq. (9). Indeed, the sample Nb10 exhibits the best metallic properties and consequently a larger contribution of the Boltzmann term is expected.

As the temperature is increased above 13 K the weak antilocalization contribution starts to dominate. This results in a positive slope of $R(T)$ (see the extrapolation curve from Eq. (9) in Fig. 6(b)). However, in comparison with the experiment the calculated transition is shifted to somewhat higher temperatures. This discrepancy indicates that in the considered range a mechanism with positive $R(T)$ slope, e.g. the Boltzmann term, is essential in all samples.

We associate the high-temperature maximum in $R(T)$ (a "bulge" in Nb10) with the emergence of the weak localization with increasing temperature so that $\tau_\varphi^{-1} \gg \tau_{so}^{-1}$. In this case the temperature dependence of the resistance is described by the formula

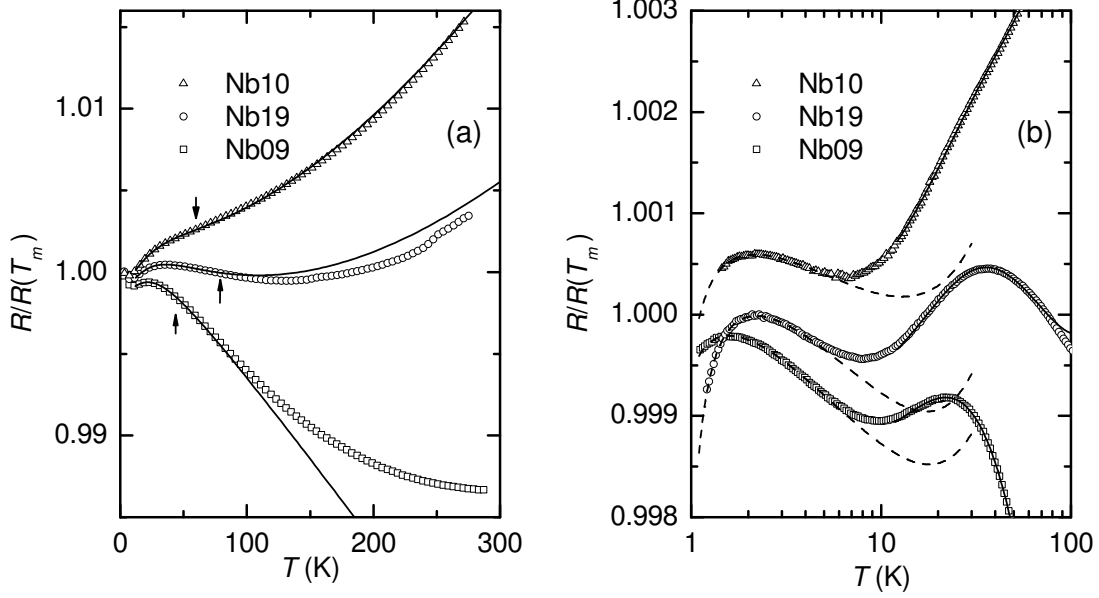


FIG. 6: The resistance vs. temperature in the linear (the left panel) and in the logarithmic (the right panel) temperature scales for samples Nb09, Nb10, and Nb19 (see TABLE I). The resistances are normalized to the value at the low-temperature maximum T_m . For better visibility curves and symbols of samples Nb09 and Nb10 are shifted vertically. The dashed lines are the best fits of the data in the range 1.2–4.2 K with Eq. (9). The solid lines are the best fits of the data with Eq. (10) in the range from 12 K to the value shown by arrows in left panel.

$$\frac{R(T)}{R(T_m)} = \frac{e^2}{2\pi^2\hbar}\rho_0 \left[-F_d\sqrt{\frac{k_B T}{\hbar D}} - 3\sqrt{\frac{1}{4\tau_{so}D} + \frac{1}{4\tau_\varphi(T)D}} + \sqrt{\frac{1}{4\tau_\varphi(T)D}} \right] + LT^p + R_0, \quad (10)$$

where the extrapolation of the low-temperature behavior of the electron-electron interaction in the diffusion channel (the first term) and the weak localization and antilocalization⁴³ (the second and third terms) is used. The Boltzmann transport term is described by the term LT^p and the superconducting fluctuation effects are ignored. The solid lines in Fig. 6 represent the best fit with Eq. (10) with parameters L , p , R_0 , and a universal $\tau_{so}^{-1} = 2.3 \times 10^{12} \text{ s}^{-1}$ for all samples. It can be seen that Eq. (10) gives a good approximation for the feature around 20–40 K and extrapolates to higher temperatures reproducing both "metallic" and "insulating" behavior. In all cases the temperature exponent of the Boltzmann term lies in the range $p = 1.2\text{--}1.4$ (see Table I). This finding points to non-Fermi-liquid behavior of conduction electrons in $\text{Nb}_{5-\delta}\text{Te}_4$. Usually the quantum interference of conduction electrons in disordered conductors is considered as a low-temperature effect. Its extension to higher temperatures is possible when the dephasing length is still larger than the electron mean free path,

$\sqrt{D\tau_\varphi} \gg \ell$. This occurs in systems with strong potential scattering such as Ti-Al alloys⁴⁴, Mo/Si multilayers⁴⁵, and ion-implanted polymers⁴⁶, where the interference effects persist above 250 K. Therefore in $\text{Nb}_{5-\delta}\text{Te}_4$, which is also characterized by a short mean free path, high-temperature quantum interference of conduction electrons is also possible.

In summary, we studied the dependence of the resistance on the magnetic field and temperature in $\text{Nb}_{5-\delta}\text{Te}_4$ single crystals with $\delta = 0.23$. The compound is a superconductor with $T_c = 0.7\text{--}0.9$ K. Both the magnetoresistance and the temperature dependence of the resistivity are quantitatively well described in the framework of the theory of quantum interference effects in disordered conductors. The electron dephasing times extracted from the magnetoresistance are determined by the electron-phonon interaction and scattering on magnetic impurities.

Acknowledgments

The authors thank V. Duppel for the microprobe analysis, E. Brücher for magnetic susceptibility measure-

ments, and D. Martien for assisting the heat capacity investigations. This work was supported by the Estonian Science Foundation Grant No. 5033. ASt kindly acknowledges support from the Max-Planck-Gesellschaft.

-
- * Electronic address: yas@fi.tartu.ee
- † Present address: Research Institute for Electronics Science, Hokkaido University, Sapporo 060-0812, Japan.
- ¹ B. L. Altshuler and A. G. Aronov, in *Electron-Electron Interactions in Disordered Systems*, edited by M. Pollak and A. M. Efros (North-Holland, Amsterdam, 1985).
 - ² Y. Imry, *Introduction to Mesoscopic Physics* (Oxford University Press, Oxford, 2002).
 - ³ B. L. Altshuler, A. G. Aronov, and D. E. Khmelnitskii, J. Phys. C: Solid State Physics **15**, 7367 (1982).
 - ⁴ J. J. Lin and L. Y. Kao, J. Phys.: Condens. Matter **13**, L119 (2001).
 - ⁵ P. Mohanty, E. M. Q. Jariwala, and R. A. Webb, Phys. Rev. Lett. **78**, 3366 (1997).
 - ⁶ M. A. Skvortsov, A. I. Larkin, and M. V. Feigel'man, Phys. Rev. Lett. **92**, 247002 (2004).
 - ⁷ J. J. Lin and J. P. Bird, J. Phys.: Condens. Matter **14**, R501 (2002).
 - ⁸ F. Pierre, A. B. Gougam, A. Anthore, H. Pothier, D. Esteve, and N. O. Birge, Phys. Rev. B **68**, 085413 (2003).
 - ⁹ Y. L. Zhong, J. J. Lin, and L. Y. Kao, Phys. Rev. B **66**, 132202 (2002).
 - ¹⁰ A. Sergeev and V. Mitin, Phys. Rev. B **61**, 6041 (2000).
 - ¹¹ J. J. Lin, Y. L. Zhong, and T. J. Li, Europhys. Lett. **57**, 872 (2002).
 - ¹² K. Selte and A. Kjekshus, Acta Chem. Scand. **17**, 2560 (1963).
 - ¹³ M. He, A. Simon, and V. Duppel, Z. Anorg. Allg. Chem. **630**, 535 (2004).
 - ¹⁴ R. Dronskowski, Ph.D. thesis, Uni. Stuttgart (1990).
 - ¹⁵ K. Tsukuma, M. Shimada, M. Koizumi, and H. Kawamura, Phys. Status Solidi A **65**, K179 (1981).
 - ¹⁶ K. Selte and A. Kjekshus, Acta Chem. Scand. **19**, 258 (1965).
 - ¹⁷ F. Hulliger, Structure and Bonding **4**, 83 (1968).
 - ¹⁸ R. Dronskowski, A. Simon, and P. Plambeck-Fischer, Zeitschrift für Kristallogr. **198**, 101 (1992).
 - ¹⁹ W. L. McMillan, Phys. Rev. **167**, 331 (1968).
 - ²⁰ P. G. de Gennes, *Superconductivity of Metals and Alloys* (W. A. Benjamin, New York Amsterdam, 1966).
 - ²¹ A. Kawabata, J. Phys. Soc. Japan **49**, 628 (1980).
 - ²² B. L. Altshuler, A. G. Aronov, A. I. Larkin, and D. E. Khmelnitskii, Zh. Eksp. Teor. Fiz. **81**, 768 (1981) [Sov. Phys. JETP **54**, 411 (1981)].
 - ²³ D. V. Baxter, R. Richter, M. L. Trudeau, R. W. Cochrane, and J. O. Strom-Olsen, J. Phys. France **50**, 1673 (1989).
 - ²⁴ A. I. Larkin, Pis'ma Zh. Eksp. Teor. Fiz. **31**, 239 (1980) [JETP Lett. **31**, 219 (1980)].
 - ²⁵ J. M. B. Lopes dos Santos and E. Abrahams, Phys. Rev. B **31**, 172 (1985).
 - ²⁶ W. Brenig, J. Low Temp. Phys. **60**, 297 (1985).
 - ²⁷ K. Meiners-Hagen and W. Gey, Phys. Rev. B **63**, 052507 (2001).
 - ²⁸ P. A. Lee and T. V. Ramakrishnan, Rev. Mod. Phys. **57**, 287 (1985).
 - ²⁹ W. B. Jian, C. Y. Wu, Y. L. Chuang, and J. J. Lin, Phys. Rev. B **54**, 4289 (1996).
 - ³⁰ M. E. Gershenson, V. N. Gubankov, and Y. E. Zhuravlev, Zh. Eksp. Teor. Fiz. **85**, 287 (1983) [Sov. Phys.-JETP **58**, 167 (1983)].
 - ³¹ C. Y. Wu and J. J. Lin, Phys. Rev. B **50**, 385 (1994).
 - ³² K. S. Il'in, N. G. Ptitsina, A. V. Sergeev, G. N. Gol'tsman, E. M. Gershenson, B. S. Karasik, E. V. Pechen, and S. I. Krasnovobodtsev, Phys. Rev. B **57**, 15623 (1998).
 - ³³ J. J. Lin, T. J. Li, and T. M. Wu, Phys. Rev. B **61**, 3170 (2000).
 - ³⁴ B. L. Altshuler and A. G. Aronov, JETP Lett. **30**, 482 (1979) [Pis'ma Zh. Eksp. Teor. Fiz. **30**, 514 (1979)].
 - ³⁵ B. L. Altshuler and A. G. Aronov, Solid State Commun. **38**, 11 (1981).
 - ³⁶ M. B. Maple, *Magnetism*, edited by H. Suhl (Academic, New York, 1973), Vol. 5.
 - ³⁷ G. Boate, G. Gallinaro, and C. Rizzuto, Phys. Rev. **148**, 353 (1966).
 - ³⁸ J. M. Gordon, C. J. Lobb, and M. Tinkham, Phys. Rev. B **29**, R5232 (1984).
 - ³⁹ C. Y. Wu, W. B. Jian, and J. J. Lin, Phys. Rev. B **57**, 11232 (1998).
 - ⁴⁰ A. Stolovits, A. Sherman, K. Ahn, and R. K. Kremer, Phys. Rev. B **62**, 10565 (2000).
 - ⁴¹ Z. Ovadyahu, Phys. Rev. B **63**, 235403 (2001).
 - ⁴² M. Yu. Reizer, Phys. Rev. B **45**, 12949 (1992).
 - ⁴³ H. Fukuyama and K. Hoshino, J. Phys. Soc. Jpn. **50**, 2131 (1981).
 - ⁴⁴ J. J. Lin and C. Y. Wu, Phys. Rev. B **48**, 5021 (1993).
 - ⁴⁵ E. I. Buchstab, A. V. Butenko, N. Y. Fogel, V. G. Cherkasova, and R. L. Rosenbaum, Phys. Rev. B **50**, 10063 (1994).
 - ⁴⁶ G. Du, V. N. Prigodin, A. Burns, J. Joo, C. S. Wang, and A. J. Epstein, Phys. Rev. B **58**, 4485 (1998).